THE JOURNAL OF PHYSICAL CHEMISTRY B
A JOURNAL OF THE AMERICAN CHEMICAL SOCIETY

pubs.acs.org/JPCB

Article

Trajectory-Extending Kinetic Monte Carlo Simulations to Evaluate Pure and Gas Mixture Diffusivities through a Dense Polymeric Membrane

Subhadeep Dasgupta, Arun K. S., K. Ganapathy Ayappa, and Prabal K. Maiti*

Cite This: *J. Phys. Chem. B* 2023, 127, 9841−9849

Read Online

ACCESS | Metrics & More | Article Recommendations | Supporting Information

ABSTRACT: With renewed interest in CO_2 separations, carbon molecular sieving (CMS) membrane performance evaluation requires diffusion coefficients as inputs to have a reliable estimate of the permeability. An optimal material is desired to have both high selectivity and permeability. Gases diffusing through dense CMS and polymeric membranes experience extended subdiffusive regimes, which hinders reliable extraction of diffusion coefficients from mean squared displacement data. We improve the sampling of the diffusive landscape by implementing the trajectory-extending kinetic Monte Carlo (TEKMC) technique to efficiently extend molecular dynamics (MD) trajectories from ns to μs time scales. The obtained self-diffusion coefficient of pure CO_2 in CMS membranes derived from a 6FDA/BPDA-DAM precursor polymer melt is found to linearly increase from 0.8−1.3 × 10^{-6} cm^2 s^{-1} in the pressure range of 1−20 bar, which supports previous experimental findings. We also extended the TEKMC algorithm to evaluate the mixture diffusivities in binary mixtures to determine the permselectivity of CO_2 in CH_4 and N_2 mixtures. The mixture diffusion coefficient of CO_2 ranges from 1.3−7 × 10^{-6} cm^2 s^{-1} in the binary mixture CO_2/CH_4, which is significantly higher than the pure gas diffusion coefficient. Robeson plot comparisons show that the permselectivity obtained from pure gas diffusion data is significantly lower than that predicted using mixture diffusivity data. Specifically, in the case of the CO_2/N_2 mixture, we find that using mixture diffusivities led to permselectivities lying above the Robeson limit highlighting the importance of using mixture diffusivity data for an accurate evaluation of the membrane performance. Combined with gas solubilities obtained from grand canonical Monte Carlo (GCMC) simulations, our work shows that simulations with the TEKMC method can be used to reliably evaluate the performance of materials for gas separations.

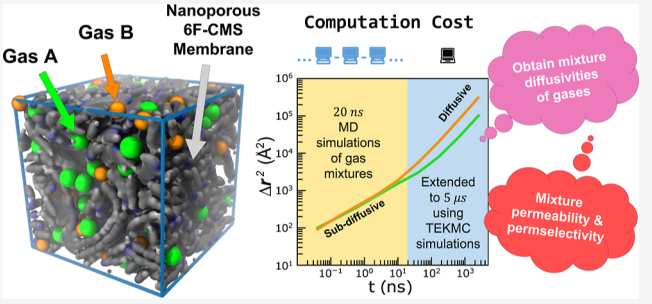

INTRODUCTION

Separating CO_2 from natural gas streams primarily involves the separation of CO_2 from gas mixtures. Separation technologies are largely comprised of solvent-based extraction techniques, cryogenic distillation, and membrane-based separations.[1] Solvent-based extraction techniques, like amine filtration, exhibit long term environmental concerns regarding energy consumption, operating challenges, and emission of hazardous byproducts.[2] Currently, industrial applications are dominated by cryogenic distillation. However, it has serious drawbacks pertaining to high energy requirements and high operating costs.[3] Membrane-based gas separation offers significant advantages due to increased stability and scalability, with the potential to improve performance based on the synthesis of novel materials while being relatively hazard free.[4] Carbon-based membranes have shown a lot of promise for effectively separating CO_2 from natural gas streams. Carbon molecular sieving (CMS) membranes are carbon-based high-performance gas separation membranes derived from the pyrolysis of polymeric precursors in vacuum or an inert atmosphere. CMS membranes present a bimodal pore size distribution and a rich network of interconnected micropores (∼0.7−2 nm) and ultramicropores (<0.7 nm) that can differentiate between pairs of gas molecules having similar kinetic diameters.[5−8] Similar pore network topologies are observed in a variety of other polymeric membranes, enabling one to modify membranes by varying the chemistry and processing conditions.[9] Membrane-based technologies also have the advantage of excellent gas selectivity with high gas permeabilities and chemical and thermal stability.[10,11] CMS membranes show great promise in carbon capture and storage applications, with their monomer composition and choice of precursor playing an important role in determining their gas adsorption and selectivity performances.

Received: August 22, 2023
Revised: October 25, 2023
Accepted: October 25, 2023
Published: November 7, 2023

https://doi.org/10.1021/acs.jpcb.3c05661
J. Phys. Chem. B 2023, 127, 9841−9849

Molecular simulations are widely used to study gas adsorption and separation processes. Grand canonical Monte Carlo (GCMC) simulations have been used to obtain adsorption isotherms for a variety of molecules and microporous materials such as metal organic frameworks (MOFs), zeolites, and carbon-based materials. These simulations are carried out under equilibrium conditions. In contrast, the transport mechanism of gases inside membranes occurs in nonequilibrium conditions across an applied pressure gradient between the upstream feed gas to be separated and the downstream gas. In this regard, polymeric membranes have been widely studied for effective CO_2 separations. Gas transport through dense polymer membranes is generally modeled by the sorption-diffusion mechanism.[12−14] Gas molecules first adsorb in the membrane under the upstream conditions, diffuse under the influence of a chemical potential gradient, and finally desorb from the membrane at the downstream compartment. The diffusive flux of the gas molecule through the membrane is measured using its permeability

$$\mathcal{P}=SD \tag{1}$$

where S and D are the solubility and diffusion coefficients of the gas molecule, respectively, in the membrane.[15] High permeability values can be achieved by increasing either D or S or both D and S. If the upstream pressure is much larger than the downstream pressure, then the solubility S can be obtained from an equilibrium GCMC simulation evaluated under the thermodynamic conditions at the upstream pressure. Molecular dynamics (MD) simulations have been widely used to evaluate the diffusion coefficient, D, in a variety of microporous materials.[16−20] Due to the complex porous networks present in glassy polymeric membranes and their derivatives, there is a drastic slowing down of the dynamics of the diffusing species. As a result, carrying out all-atom MD simulations to adequately sample the diffusive regime and reliably evaluate D is a computational challenge. Alternate approaches have been devised to overcome this limitation with the primary goal of evaluating the self-diffusion coefficients of slowly diffusing gas species. Thornton et al. presented an approximate dependence of gas diffusivity on the fractional free volume of the porous media and the kinetic diameter of the gas, derived empirically from available experimental data.[21] Bousige et al. analyzed the residence and relocation times of fluid in ultraconfining disordered porous materials by mapping MD simulations to mesoscopic random walks.[22] Neyertz and Brown proposed a variant of kinetic Monte Carlo (kMC), referred to as trajectory-extending kinetic Monte Carlo (TEKMC).[23] The algorithm has been successfully used to calculate the diffusion coefficients of small molecules such as H_2O, O_2, and N_2 in glassy polymers.[23,24]

While assessing a given material for a particular gas separation technology, both solubility and diffusion coefficients in a gas mixture need to be evaluated. The gas solubility can be obtained from mixture GCMC simulations; however, evaluating the diffusion coefficients of mixtures is more challenging.[25,26] There are several reports of computing gas permeabilities in polymers, metal organic frameworks, and zeolites using both pure and mixture gas data while comparing them with the Robeson upper limit (RUL)[27,28] where higher selectivity is correlated with lowered permeability. These plots are used as a standard to assess the performance of newly fabricated adsorbents, where the goal is to design a material with both high selectivity and permeability. There are also ongoing efforts to redefine and increase the upper limits for different materials.[29−31] With a wide range of data available, machine learning techniques have also been leveraged to understand and find materials that can surpass the Robeson upper bounds.[32] Recent attempts to address mixture diffusivities from MD simulations showed that gas molecules tend to oscillate between adsorption sites,[33] making it difficult to evaluate the long time gas diffusivity. Since the evaluation of diffusion coefficients in mixtures is challenging, several studies have evaluated the permeabilities using pure component diffusion coefficients. Semiempirical approaches have been developed with varying degrees of success to obtain mixture diffusion coefficients from pure diffusivity data.[34] Lattice-based techniques have been used to compute the diffusion of gases inside such variable pore structures;[35,36] however, they require various parameters which are difficult to determine. In this work, to overcome these limitations, we extend the TEKMC technique to reliably obtain the mixture diffusivities of gases inside the 6F-CMSM membrane. Robeson plot comparisons are made with permeability data obtained from both pure and mixture diffusivities to highlight the limitations of using pure component diffusivity data while designing membranes for gas separation applications.

In our previous study,[37] we modeled CMS membranes derived from a 6FDA/BPDA-DAM precursor polymer melt[38,39] (denoted as 6F-CMSM). The molecular structures were built in close correspondence with experimental compositions using density functional theory (DFT) for optimizing the two monomeric units (pyridine and pyrrole), followed by their polymerization using all-atom MD simulations. GCMC simulations were used to obtain gas adsorption isotherms inside the membrane for a range of pressures. Our simulated 6F-CMSM morphologies helped us understand the importance of the length of carbon chains in determining the density of the membrane and their accessible pore volumes, which in turn influence their adsorption performances. More details about the CMS membrane simulations can be found in our previous publication.[37] In continuation of our previous study, here, we analyze the dynamics of the adsorbed gases through the porous networks of 6F-CMSM. The solubility coefficients needed in this work are obtained from the previous gas adsorption isotherms under different pressures. Predicting accurate values of $\mathcal{P}$ requires estimating both S and D for each gas component. The novelty of our work lies in using TEKMC to obtain the self-diffusion coefficients of CO_2, CH_4, and N_2 in pure gases and the multicomponent diffusivities in binary mixtures as a function of pressure. We obtained the permeability for pure gases and binary CO_2/CH_4 and CO_2/N_2 mixtures to evaluate the membrane performance. The article is organized as follows. We have first discussed in detail the methodology used to perform the TEKMC steps. Next, we studied the variation of gas diffusivities and ultimately their permeation through 6F-CMSM. We further studied the relative permeabilities of these gases in both the pure state and binary mixtures in the 6F-CMSM polymeric membrane to understand its dependence on system pressure and gas compositions. Finally, we have presented the Robeson plots for the different systems to illustrate the importance of using accurate mixture diffusion coefficients while assessing a material's capacity for separating a given gas mixture.

https://doi.org/10.1021/acs.jpcb.3c05661
J. Phys. Chem. B 2023, 127, 9841−9849

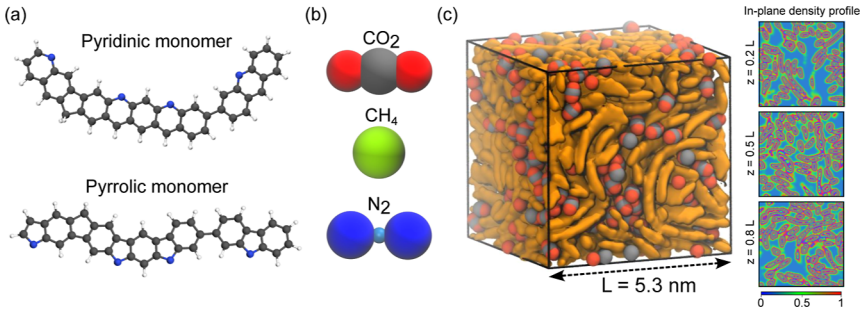

Figure 1. (a) Atomic structures of pyridinic and pyrrolic monomer fragments that cross-link and polymerize to form the derived 6F-CMSM. Gray denotes carbon, blue denotes nitrogen, and white denotes hydrogen atoms. (b) Atomic structure for the three gases considered in this work based on the TraPPE force field. Three-site CO_2 is modeled with two oxygen (red) and one carbon (gray) atoms. CH_4 is represented by a united atom model, having a single bead (green). The three-site N_2 with two nitrogen atoms (blue) and one fictitious center of mass bead (cyan). (c) Snapshot showing the derived 6F-CMSM containing adsorbed CO_2 in the pores, corresponding to T = 308 K and P = 20 bar. The surfaces of the cross-linked monomers are colored orange. Shown on the right are in-plane density profiles for three cross sections. The blue regions represent the pores, and the green to red regions denote the presence of 6F-CMSM atoms. The difference in porous structure across the z-plane indicates the formation of complex network pathways along the bulk of 6F-CMSM. These interconnected pores govern the dynamics and diffusion of gases inside 6F-CMSM.

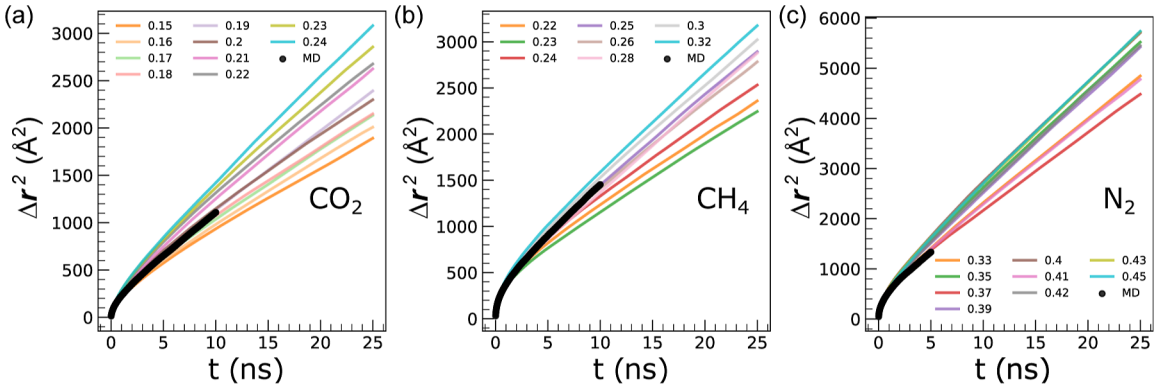

Figure 2. Mean squared displacement (Δr^2) of (a) CO_2, (b) CH_4, and (c) N_2 inside 6F-CMSM at a temperature of 308 K and 20 bar pressure. The thick black line shows the values obtained from the all-atom MD simulations. The finer colored lines show the values obtained from 50 ns TEKMC simulations for different values of d_{grid} (nm). The values of d_{grid} are tuned to obtain an MSD with the least mean squared error *w.r.t.* the values obtained from the MD simulation.

METHODS

Computational Modeling and Simulation. The 6F-CMSM used in this work is composed of pyridinic and pyrrolic monomer units, as shown in Figure 1a. These monomers polymerize to form various morphologies, among which we select the structure that yields the closest match with experimental gas adsorption isotherms as discussed in our earlier work.[37] The structures of CO_2, CH_4, and N_2 molecules used are shown in Figure 1b. The interactions involving the gas molecules are modeled using the TraPPE force fields[40] and the 6F-CMSM atoms are modeled using the modified Dreiding force field.[38,41] The force field values used in this work are reported in Table S1 of the Supporting Information. The distribution of gas molecules inside 6F-CMSM is obtained from GCMC simulations as discussed in our earlier work. To account for the structural rearrangement of monomer constituents upon interaction with gas molecules, 6F-CMSM is modeled as a flexible membrane. We first perform all-atom MD simulations of 6F-CMSMs along with the adsorbed gases for 20 ns duration in an *NVT* ensemble using LAMMPS.[42] The temperature of the system is maintained at 308 K using a Nosé−Hoover thermostat. The coordinates of the gas molecules from the MD simulation are stored at intervals of τ_{MD} = 10 ps. Figure 1c shows a snapshot from our all-atom MD simulation of 6F-CMSM loaded with CO_2 corresponding to a 20 bar pressure. The porous nature of the membrane for different cross sections along the bulk of the membrane is also visible from the simulation snapshot.

Implementing Kinetic Monte Carlo. The simulation box is uniformly divided into voxels of grid size (d_{grid}) along the x, y, and z directions. Each voxel is identified by a single index, spanning from 1 to $n_{voxel} = (L/d_{grid})^3$, for a cubic simulation box having length L on each side. All gas molecules are mapped from their real-space (x, y, and z) coordinates to their respective voxel indices. The trajectories of the gas molecules from the MD simulations are used to compute the transition probability matrix (π_{ij}) required as input for the TEKMC simulation. We define the probability of transition between voxels i and j, given that the gas is in voxel i as

$$\pi_{ij} = \frac{N_{ij}}{N_i} \tag{2}$$

where N_{ij} is the number of transitions between voxels i and j and N_i is the number of times the gas molecule visits voxel i. Since the transition probability matrix is constructed from the all-atom MD trajectories, π_{ij} implicitly takes into account all of the gas−gas and gas−membrane interactions. The probability matrix is symmetrized to maintain detailed balance, such that $\pi_{ij} = \pi_{ji}$, which is equivalent to

https://doi.org/10.1021/acs.jpcb.3c05661
J. Phys. Chem. B 2023, 127, 9841−9849

$$N_{ij} = N_{ji} = (N'_{ij} + N'_{ji})/2 \quad (3)$$

where N_{ij}' and N_{ji}' are the recorded number of transitions from voxel i to j and j to i, respectively. Voxels with $\pi_{ii} = 0$ indicate regions inside the simulation box where the atoms of the CMS molecules are located. The values of π_{ii} for CO_2, CH_4, and N_2 for 1 and 20 bar pressures are shown in Figure S1 of the Supporting Information. In the case of binary gas mixtures, π of each component is obtained from the trajectory of that component. The interaction between two components changes the probability distribution in the pure gas system, as shown in Figure S2 of the Supporting Information for 20 bar pressure. From the conservation of the number of particles, we have the condition $\Sigma_j \pi_{ij} = 1, \forall i$. For each kMC move, a walker is placed randomly in one of the visited voxels i such that $\pi_{ii} \neq 0$. The voxel j that the walker visits from i is determined from the sum, $\sigma(j') = \Sigma_1^{j'} \pi_{ij}$. The destination voxel is identified to be $j = j'$ when $\sigma(j') \geq r$ is satisfied, where r is a random number drawn from a uniform distribution. A total of 5000 random walkers are inserted for each simulation, and the time associated with each kMC step is τ_{kMC}. The trajectories of these random walkers are mapped back from the voxel index to the real space coordinates, and their average mean squared displacement (MSD) is determined.

Optimization to Obtain Diffusion and Permeability. The optimal values of τ_{MD} and d_{grid} combinations first need to be determined for obtaining the correct MSD from the TEKMC simulation. Different techniques can be used to obtain the time interval between two successive kMC steps, τ_{kMC}.[43] We follow the procedure prescribed by Neyertz et al., where $\tau_{kMC} = \tau_{MD}$ $(=\tau)$. Figure 2 illustrates the values of MSD obtained from all-atom MD and TEKMC simulations for CO_2, CH_4, and N_2 at 20 bar pressure. For a diffusing particle, the MSD is $\langle \Delta \boldsymbol{r}(t)^2 \rangle \propto t^{\alpha}$. The value of the exponent α from the MSD data obtained from MD simulations lies in the range of 0.6−0.8, indicating the subdiffusive nature of the diffusing molecule in the polymeric membrane. In the diffusive regime where the value of $\alpha \simeq 1$, the diffusivity is obtained from the Einstein relation

$$D = \lim_{t\to\infty} \frac{1}{6t} \langle \Delta \boldsymbol{r}(t)^2 \rangle = \lim_{t\to\infty} \frac{1}{6t} \langle [\boldsymbol{r}(t + t_0) - \boldsymbol{r}(t_0)]^2 \rangle \quad (4)$$

where $\langle \cdots \rangle$ represent averages over all particles and shifted time origins (t_0). The TEKMC simulations enable us to access the Brownian regime for restricted diffusing molecules, which predominantly sample the subdiffusive regime during the small time scale of MD simulations. In order to determine the optimal value of d_{grid}, we used the lowest mean squared error (MSE) between MSDs obtained from the MD simulation and those obtained from 100 ns TEKMC simulations. The optimum values of d_{grid} for the different cases considered are shown in Table 1. To determine the diffusion coefficients, we carry out additional TEKMC simulations for three different d_{grid} values, which include the optimal d_{grid} (Table 1) as well as simulations at $d_{grid} \pm 0.01$ nm. For these three different values of d_{grid}, random walks are performed up to 5 μs to ensure all gases attain the Brownian diffusion regime, and the reported values of D are an average over these TEKMC simulations. The in-house TEKMC code developed in this study was validated by reproducing the diffusivity of bulk water and is discussed in the Supporting Information section. From TEKMC, we obtain the diffusion coefficient of SPC/E water to be $2.47 \pm 0.15 \times 10^{-5}$ cm^2 s^{-1} at 300 K, in agreement with literature.[44,45] The algorithm is generic and can be used for other systems, where such kMC algorithms are applicable.

Table 1. Optimum Values of d_{grid} (nm) Corresponding to the Lowest MSE between MSD Obtained from TEKMC and MD Simulations for the Three Gases

P (bar)	0.1	0.6	1	6	10	15	20
CO_2	0.41	0.32	0.22	0.19	0.20	0.20	0.20
CH_4	0.61	0.42	0.34	0.30	0.32	0.24	0.25
N_2	0.60	0.55	0.47	0.45	0.44	0.35	0.33

The solubility coefficient of the i^{th} gas species (S_i) in a membrane is the ratio between its volumetric loading $V_{L,i}$ and its partial pressure p_i at a constant temperature[46]

$$S_i = \frac{V_{L,i}}{p_i} \quad (5)$$

The adsorption isotherm is expressed in terms of the volumetric loading as

$$V_{L,i} = \frac{N_i(T, P)}{V_{CMS}} \frac{k_B T_{STP}}{P_{STP}} \quad (6)$$

where $N(T, P)$ is the number of gas molecules adsorbed in the 6F-CMSM membrane at temperature T and pressure P, V_{CMS} is the volume of the 6F-CMSM membrane, k_B is the Boltzmann constant, and T_{STP} and P_{STP} correspond to the standard temperature and pressure, respectively. The equilibrated values of V_L were obtained using the Peng−Robinson equation of state[47] implemented in RASPA,[48] detailed in our previous work.[37] The solubility coefficients can be estimated accurately using the above equations, ultimately allowing us to compute their corresponding permeabilities.

RESULTS AND DISCUSSION

Gas Dynamics inside 6F-CMSM. Figure 3a shows the averaged MSD $(\Delta \boldsymbol{r}^2)$ of CO_2, CH_4, and N_2 for the entire range of system pressures obtained from 5 μs TEKMC simulations and the corresponding values of the exponent α are illustrated in Figure 3b. The time taken to attain the Brownian regime for the three gases is significantly higher at low pressures compared to the time taken at higher pressures. We observe a slow growth of the exponent toward $\alpha = 1$, and the Brownian regime is observed above a sampling time of 1 μs. The inset in Figure 3a illustrates two representative trajectories for CO_2 molecules corresponding to 0.1 and 20 bar pressures. At low pressures (0.1 bar), gas molecules remain trapped in higher energy adsorption sites restricting displacements to a small region of the CMS membrane and resulting in a subdiffusive nature of the MSD ($\alpha < 0.7$) even after 5 μs. At higher pressures, a distinct crossover from subdiffusive to diffusive regimes is observed. We note that at higher pressures, increased gas uptake results in the swelling of 6F-CMSM giving rise to flexible permeation pathways.[37]

The diffusion coefficients obtained from the Brownian regimes, ($\alpha \simeq 1$), for different pressures are shown in Figure 4a. In literature, the experimentally reported value of D for CO_2 inside 6F-CMSM derived from 6FDA/BPDA-DAM pyrolyzed at 550 °C is 1.32×10^{-6} cm^2 s^{-1}.[49] Our calculated value of D_{CO_2} is in excellent agreement with the experimental value. From the values obtained in Figure 3, the estimated time

https://doi.org/10.1021/acs.jpcb.3c05661
J. Phys. Chem. B 2023, 127, 9841−9849

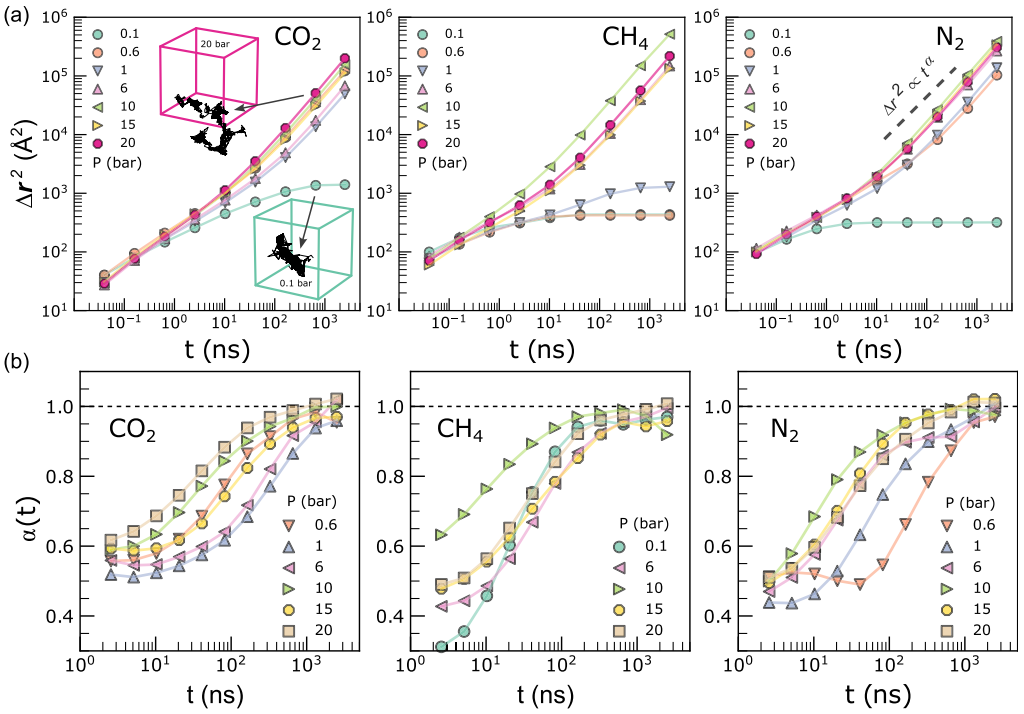

Figure 3. (a) MSD (Δr^2) versus time for different gases CO_2, CH_4, and N_2. The dynamics of the gas molecules vary significantly depending on the system pressure (indicated by the different colors shown in the legend). The inset shows two sample, unwrapped trajectories of a walker representing CO_2 molecules inside 6F-CMSM at 0.1 and 20 bar pressures obtained from kMC. (b) The growth of the MSD exponent (α) versus time for the three gases is presented for systems that attain the Brownian regime successfully. The dashed line shows the reference level of $\alpha = 1$. The time taken to reach $\alpha = 1$ decreases with increasing pressure.

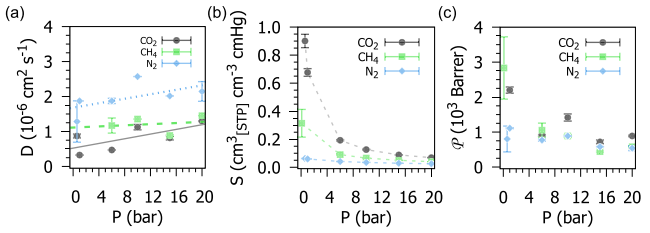

Figure 4. Dependence of (a) self-diffusion coefficient, D; (b) solubility coefficient, S; and (c) permeability, $\mathcal{P}$, of pure CO_2, CH_4, and N_2 adsorbed inside 6F-CMSM for increasing pressure P at T = 308 K. The data shown are averaged over independent kMC simulations using the three best grid sizes for each pressure point.

scale for obtaining a diffusive regime at pressure P = 20 bar is around 500 ns for CO_2. For cross-validation against all-atom MD results, we performed an additional all-atom MD simulation of 500 ns. The diffusion coefficient from the all-atom MD $\sim 1.23 \times 10^{-6}$ cm^2 s^{-1}. Both the experimental and all-atom MD values are close to the converged value obtained using TEKMC. This remarkable agreement further allows us to conclude that the algorithm can successfully extrapolate short MD results to a longer duration and can be successfully used for computing the diffusion of confined gas molecules. We also observe that a sufficient number of percolating pathways are required during the atomistic MD simulation in order to adequately access all possible pores available for the gas molecules to diffuse through. From the dependence of D on P, in Figure 4a, we observe a weak linear increase in the diffusivities of all three gases inside 6F-CMSM as a function of pressure. The loading-dependent diffusion coefficients have been observed for hydrocarbons in metal organic frameworks,[17] which lead to structural changes of the adsorbing framework.[50] There is a monotonic increase of D in the pressure range studied for all gases, which is nontrivial and to the best of our knowledge not reported earlier for CMS membranes. We observe that N_2 diffuses faster than CO_2 inside 6F-CMSM, which is similar to the diffusive nature inside zeolites reported in literature.[18]

Solubility and Permeability of Pure Gases. The solubilities (S) of CO_2, CH_4, and N_2 versus pressure for 6F-CMSM corresponding to temperature 308 K using the values of V_L from our previous study of gas uptake in 6F-CMSM[37] calculated using eq 5 are shown in Figure 4b. The values of S for CO_2 are the highest followed by CH_4. N_2 solubilities are the lowest and are independent of pressure. We observe a monotonic decrease in the solubility coefficient with an increase in pressure for all gases inside 6F-CMSM. Permeability ($\mathcal{P}$) is then obtained using eq 1 in units of Barrer, as shown in Figure 4c. In general, the permeability values for CO_2 are the highest when compared with those of CH_4 and N_2. We also observe that the permeability decreases with pressure with the most noticeable variation seen in CO_2 and CH_4, and the effect is less pronounced for N_2. The linear growth of D with P signifies that any variation in $\mathcal{P}$ is strongly dominated by S.

Permselectivity in Binary Gas Mixtures. In order to understand the relative permeability of different gases inside 6F-CMSM, we also compute the permselectivity ($\alpha_{\mathcal{P}}$) of CO_2 in binary gas mixtures of CO_2/CH_4 (50:50 and 10:90) and CO_2/N_2 (20:80). The permselectivity of a gas mixture is given by

https://doi.org/10.1021/acs.jpcb.3c05661
J. Phys. Chem. B 2023, 127, 9841−9849

Table 2. Diffusion Coefficients, Solubility, and Permeability of Each Species for Different Binary Gas Mixtures inside 6F-CMSM

P (bar)	D_i (10^{-6} cm^2 s^{-1})		S_i (10^{-2} cm$_{[STP]}^3$ cm^{-3} cmHg)		$\mathcal{P}_i$ (10^3 Barrer)	
			CO_2/CH_4 (50:50)			
	CO_2	CH_4	CO_2	CH_4	CO_2	CH_4
4	1.34 ± 0.12	0.78 ± 0.26	39.96 ± 3.00	4.85 ± 0.76	5.34 ± 0.61	0.38 ± 0.14
6	1.65 ± 0.20	0.50 ± 0.13	29.78 ± 2.22	3.59 ± 0.56	4.91 ± 0.69	0.18 ± 0.06
10	3.35 ± 0.14	4.75 ± 0.83	20.09 ± 1.49	2.35 ± 0.38	6.72 ± 0.58	1.12 ± 0.27
15	3.42 ± 0.44	4.24 ± 0.78	14.36 ± 1.03	1.68 ± 0.26	4.91 ± 0.72	0.71 ± 0.11
20	7.02 ± 0.67	13.55 ± 0.78	11.22 ± 0.78	1.27 ± 0.20	7.88 ± 0.93	1.73 ± 0.28
			CO_2/CH_4 (10:90)			
	CO_2	CH_4	CO_2	CH_4	CO_2	CH_4
4	2.07 ± 0.07	0.73 ± 0.26	78.28 ± 28.29	8.55 ± 0.80	16.16 ± 5.87	0.62 ± 0.23
6	5.87 ± 0.35	7.25 ± 0.52	61.31 ± 19.76	6.61 ± 0.56	35.99 ± 11.80	4.80 ± 0.53
10	5.4 ± 0.43	9.92 ± 0.53	43.21 ± 10.66	4.62 ± 0.3	23.31 ± 6.04	4.59 ± 0.39
15	2.12 ± 0.20	1.47 ± 0.13	32.34 ± 7.76	3.41 ± 0.22	6.87 ± 1.77	0.50 ± 0.06
20	7.41 ± 0.36	12.90 ± 0.82	26.01 ± 5.64	2.70 ± 0.16	19.27 ± 4.28	3.48 ± 0.30
			CO_2/N_2 (20:80)			
	CO_2	N_2	CO_2	N_2	CO_2	N_2
4	1.50 ± 0.12	3.00 ± 0.45	71.91 ± 7.66	2.03 ± 0.49	10.77 ± 1.44	0.61 ± 0.17
6	2.14 ± 0.19	2.80 ± 0.16	56.13 ± 5.41	1.58 ± 0.35	11.98 ± 1.56	0.44 ± 0.10
10	2.44 ± 0.16	2.11 ± 0.19	39.59 ± 3.53	1.14 ± 0.23	9.65 ± 1.07	0.24 ± 0.05
15	1.44 ± 0.08	2.27 ± 0.22	29.57 ± 2.47	0.86 ± 0.02	4.26 ± 0.43	0.20 ± 0.04
20	2.35 ± 0.16	3.18 ± 0.22	23.81 ± 2.00	0.67 ± 0.01	5.59 ± 0.60	0.21 ± 0.04

$$\alpha_{\mathcal{P}} = \frac{\mathcal{P}_X}{\mathcal{P}_Y} \tag{7}$$

where X denotes CO_2 and Y denotes CH_4 or N_2, depending on the composition of the gas mixture. The diffusion coefficients of gas molecules are influenced by their interactions with the membrane as well as with neighboring gas molecules. Consequently, the diffusion coefficient of each component in a mixture deviates from the corresponding pure gas diffusion coefficients. The deviation is nontrivial, and there is an ongoing effort to understand multicomponent gas diffusion in different adsorbing frameworks.[16,18,19,51,52] To address this challenge, we extended the TEKMC simulations to gas mixtures of different compositions. The probability matrix for the binary gas mixture is created by tracking the positions of individual gas species during the MD runs, as was done for the pure single-component system described earlier. We performed separate TEKMC simulations for each species in the binary gas mixture system to obtain the corresponding mixture diffusion coefficients for each component in the mixture. The TEKMC optimization was also carried out independently for each mixture at different pressures to obtain the diffusivities. This data is obtained from 5 μs long TEKMC simulations, and the diffusivities were computed from the MSD data over 2.5 μs to sample the Brownian diffusive regime (Figure S3). For the binary mixtures, the permeability $\mathcal{P}_i$ for the ith component is obtained from the corresponding solubility S_i. S_i values are obtained using eq 5, from binary mixture GCMC simulations reported in our previous work.[37] The corresponding values of D_i, S_i, and $\mathcal{P}_i$ for the different gas mixtures are given in Table 2. The variations of the diffusive exponent α for the mixtures are illustrated in Figure S3 of the Supporting Information. We observe that the diffusivities of CO_2, CH_4, and N_2 in their binary mixtures deviate significantly from the pure component values. D_{CO_2} is greater in the majority of the binary mixtures when compared to the diffusivity of pure CO_2 for a given pressure value reflecting the altered energy landscape for CO_2 in the mixture. The diffusivities of both CH_4 and N_2 are higher than that of CO_2, particularly at higher pressures. The difference in the mixture diffusivities of the two species is higher for CH_4 than those of N_2. However, the high adsorption of CO_2 onto 6F-CMSM leads to significantly higher S_{CO_2}, which in turn results in a greater increase for $\mathcal{P}_{CO_2}$ when compared with CH_4 and N_2. We also note a decrease in the diffusivities for CO_2/CH_4 (10:90) at a pressure of 15 bar; however, the reason for this particular deviation is not completely understood as the MSD data was well within the diffusive regime for both species.

Figure 5a shows the Robeson plots for different mixtures where we have used the solubility mixture data with pure component diffusivity values to obtain the permeabilities. In Figure 5b, mixture data (Table 2) were used for both the solubilities and diffusivities. The RUL for different CO_2/CH_4 and CO_2/N_2 is plotted for comparison.[27] Upon comparing

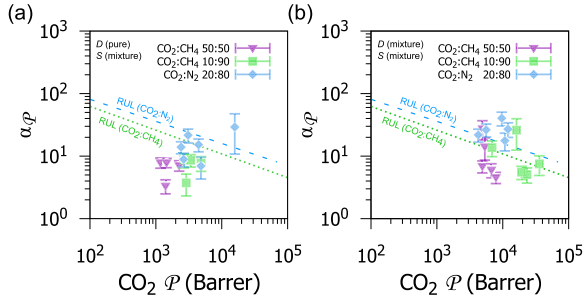

Figure 5. (a) Permselectivity ($\alpha_{\mathcal{P}}$) calculated using diffusion (D) from pure gas simulations and solubility (S) from binary gas mixtures inside 6F-CMSM. (b) $\alpha_{\mathcal{P}}$ calculated using both D and S from binary gas mixtures. $\mathcal{P}$ and $\alpha_{\mathcal{P}}$ computed from binary gas simulations are higher than those from pure gas simulations. The dashed lines correspond to the RUL for different gases.[27] $\alpha_{\mathcal{P}}$ obtained from mixture simulations are significantly higher than that from pure simulation values.

https://doi.org/10.1021/acs.jpcb.3c05661
J. Phys. Chem. B 2023, 127, 9841−9849

Figure 5a,b, we first note that both $\alpha_{\mathcal{P}}$ and $\mathcal{P}$ increase while using values for S_i and $\mathcal{P}_i$ computed from mixture data. Using pure component D_i values for the Robeson plot results in a lowering of the corresponding values, leading to underpredicting the performance of a given material. In Figure 5a, we observe a single point for the CO_2/N_2 (20:80) mixture that lies above the Robeson limit. This point corresponds to the lowest pressure of 0.6 bar, for which we did not evaluate the corresponding mixture diffusivities. Interestingly, we observe that the data for the CO_2/N_2 (20:80) mixture lies at or above the RUL when mixture diffusivity data is used (Figure 5b). Similar trends are observed for the CO_2/CH_4 (10:90) mixture as well as for CO_2/CH_4 (50:50). The increase in $\mathcal{P}_i$ for CO_2 is primarily due to the increase in the diffusivities of CO_2 in the mixtures compared to the pure gas diffusivities. The increased permselectivities, $\alpha_{\mathcal{P}}$, are due to a higher diffusivity ratio obtained with mixture diffusivities.

Our results indicate that using values of single-component gas diffusivities can lead to an underestimation of the true permselectivity of a membrane. Hence, accurate estimates of the diffusivity in both experiments and simulations are needed in order to assess the separation performance of a given material. This will also facilitate a better understanding of the RULs possessed by different membranes synthesized in the laboratory as well as from in silico predictions using MD simulations and machine learning-based predictions.[30,32] We finally point out that although we have observed these trends for a specific adsorbent, in this case, for 6F-CMSM a similar analysis would be required to assess the generality of the trends observed in this study.

CONCLUSIONS AND OUTLOOK

In this work, we obtained the permeability of CO_2, CH_4, and N_2 gases inside 6F-CMSM for different pressure conditions using multiscale computational techniques, namely, all-atom MD followed by TEKMC simulations. The dynamics of adsorbed gas molecules inside the membrane is usually retarded, leading to subdiffusive mean squared displacements in the time scales of typical all-atom MD simulations. To sample the diffusive dynamics regime, the TEKMC algorithm enables us to extend all-atom MD trajectories to 5 μs time scales where the diffusive limit can be reliably sampled. The constructed transition probability matrices also help us understand the accessible and inaccessible regions of the complex pore networks in the membrane. In a distinct departure from earlier works, we extend the TEKMC simulations to obtain the diffusion coefficients of gas mixtures. To our knowledge, this is the first time that mixture diffusivity data has been obtained using this method. For the pure components CO_2, N_2, and CH_4, we report a linear increase in the gas diffusivity confined in the 6F-CMSM matrix with an increase in pressure. Conversely, both the solubility and permeability of the gases are found to decrease with pressure.

We make a detailed comparison of the permselectivity using both pure component and mixture diffusivity data in 6F-CMSM to assess the extent of deviations observed when pure component diffusivity data are used in lieu of mixture diffusivities. The implementation of the TEKMC algorithm is available as a package on request. Gas solubility data are calculated using previous GCMC mixture simulations.[37] CO_2 diffusivities in both CH_4 and N_2 mixtures in 6F-CMSM were found to be higher than the pure component values. This leads to a significant increase in both the permselectivity and permeabilities with the use of mixture diffusivities on the Robeson plots, with data lying at or above the RUL for the CO_2/N_2 (20:80) mixtures. Our analysis indicates that for the CO_2/CH_4 and CO_2/N_2 mixtures investigated in this study, pure component diffusivities underestimate the membrane performance by varying amounts. Our findings emphasize the importance of obtaining accurate mixture diffusivity data while designing membranes for a given separation process. Coupled with GCMC and combined MD and TEKMC simulations, our study provides a complete in silico framework that can be routinely used to assess the performance of membranes for gas separation processes. We restricted our analysis to the TEKMC study of self-diffusion coefficients in order to determine the gas permeabilities for the Robeson plots to assess separation performance in the polymeric membranes. The TEKMC analysis can potentially be extended to obtain the mutual diffusion coefficients, determined from cross-correlations between different species in the mixture.[53] Correlations between species in a mixture are a function of the pore size, gas loading, and interactions between the gas and the surface. A detailed analysis is needed to fully assess the determination of transport diffusivities while evaluating the gas permeabilities in polymeric membranes.

ASSOCIATED CONTENT

Data Availability Statement

The data underlying this study are available on request. The code is available at https://github.com/PKMLab/tekmc.

Supporting Information

The Supporting Information is available free of charge at https://pubs.acs.org/doi/10.1021/acs.jpcb.3c05661.

Force field parameters, validation of the TEKMC algorithm using bulk water simulations, probability distribution of gases used for performing TEKMC, and binary component diffusion inside 6F-CMSM (PDF)

AUTHOR INFORMATION

Corresponding Author

Prabal K. Maiti − *Department of Physics, Indian Institute of Science, Bangalore 560012, India;* orcid.org/0000-0002-9956-1136; Email: maiti@iisc.ac.in

Authors

Subhadeep Dasgupta − *Department of Physics, Indian Institute of Science, Bangalore 560012, India;* orcid.org/0000-0003-1784-7016

Arun K. S. − *Department of Physics, Indian Institute of Science, Bangalore 560012, India*

K. Ganapathy Ayappa − *Department of Chemical Engineering, Indian Institute of Science, Bangalore 560012, India;* orcid.org/0000-0001-7599-794X

Complete contact information is available at: https://pubs.acs.org/10.1021/acs.jpcb.3c05661

Notes

The authors declare no competing financial interest.

ACKNOWLEDGMENTS

The authors thank the Department of Science and Technology, India, for funding and providing computational resources.

REFERENCES

(1) Carta, M. In *Encyclopedia of Membranes*; Drioli, E., Giorno, L., Eds.; Springer Berlin Heidelberg: Berlin, Heidelberg, 2015; pp 1−3.
(2) Nielsen, C. J.; Herrmann, H.; Weller, C. Atmospheric Chemistry and Environmental Impact of the Use of Amines in Carbon Capture and Storage (Ccs). *Chem. Soc. Rev.* **2012**, *41*, 6684−6704.
(3) Bhatta, L. K. G.; Subramanyam, S.; Chengala, M. D.; Olivera, S.; Venkatesh, K. Progress in hydrotalcite like compounds and metal-based oxides for CO2 capture: a review. *J. Clean. Prod.* **2015**, *103*, 171−196 Carbon Emissions Reduction: Policies, Technologies, Monitoring, Assessment and Modeling.
(4) Koros, W. J. Evolving Beyond the Thermal Age of Separation Processes: Membranes Can Lead the Way. *AIChE J.* **2004**, *50*, 2326−2334.
(5) Kamath, M. G.; Itta, A. K.; Hays, S. S.; Sanyal, O.; Liu, Z.; Koros, W. J. Pyrolysis End-Doping To Optimize Transport Properties of Carbon Molecular Sieve Hollow Fiber Membranes. *Ind. Eng. Chem. Res.* **2020**, *59*, 13755−13761.
(6) Vu, D. Q.; Koros, W. J.; Miller, S. J. High Pressure CO2/CH4 Separation Using Carbon Molecular Sieve Hollow Fiber Membranes. *Ind. Eng. Chem. Res.* **2002**, *41*, 367−380.
(7) Kumar, R.; Zhang, C.; Itta, A. K.; Koros, W. J. Highly Permeable Carbon Molecular Sieve Membranes for Efficient CO2/N2 Separation At Ambient and Subambient Temperatures. *J. Membr. Sci.* **2019**, *583*, 9−15.
(8) Rungta, M.; Wenz, G. B.; Zhang, C.; Xu, L.; Qiu, W.; Adams, J. S.; Koros, W. J. Carbon Molecular Sieve Structure Development and Membrane Performance Relationships. *Carbon* **2017**, *115*, 237−248.
(9) Song, W.; Park, J.; Dasgupta, S.; Yao, C.; Maroli, N.; Behera, H.; Yin, X.; Acharya, D. P.; Zhang, X.; Doherty, C. M.; Maiti, P. K.; Freeman, B. D.; Kumar, M. Scalable Pillar[5]Arene-Integrated Poly(Arylate-Amide) Molecular Sieve Membranes To Separate Light Gases. *Chem. Mater.* **2022**, *34*, 6559−6567.
(10) Li, L.; Xu, R.; Song, C.; Zhang, B.; Liu, Q.; Wang, T. A review on the progress in nanoparticle/C hybrid CMS membranes for gas separation. *Membranes* **2018**, *8*, 134.
(11) Williams, P. J. Analysis of Factors Influencing the Performance of Cms Membranes for Gas Separation. Ph.D. Thesis; Georgia Institute of Technology, 2006.
(12) Paul, D. The Solution-Diffusion Model for Swollen Membranes. *Sep. Purif. Methods* **1976**, *5*, 33−50.
(13) Wijmans, J. G.; Baker, R. W. The Solution-Diffusion Model: A Review. *J. Membr. Sci.* **1995**, *107*, 1−21.
(14) Lonsdale, H. The Growth of Membrane Technology. *J. Membr. Sci.* **1982**, *10*, 81−181.
(15) Suloff, E. Permeability, Diffusivity, and Solubility of Gas and Solute Through Polymers. Sorption Behavior of an Aliphatic Series of Aldehydes in the Presence of Poly(ethylene terephthalate) Blends Containing Aldehyde Scavenging Agents Wiley, 2002; pp 29−99.
(16) Skoulidas, A. I.; Sholl, D. S.; Johnson, J. K. Adsorption and Diffusion of Carbon Dioxide and Nitrogen Through Single-Walled Carbon Nanotube Membranes. *J. Chem. Phys.* **2006**, *124*, 054708.
(17) Verploegh, R. J.; Nair, S.; Sholl, D. S. Temperature and Loading-Dependent Diffusion of Light Hydrocarbons in ZIF-8 as Predicted Through Fully Flexible Molecular Simulations. *J. Am. Chem. Soc.* **2015**, *137*, 15760−15771.
(18) Selassie, D.; Davis, D.; Dahlin, J.; Feise, E.; Haman, G.; Sholl, D. S.; Kohen, D. Atomistic Simulations of CO2 and N2 Diffusion in Silica Zeolites: The Impact of Pore Size and Shape. *J. Phys. Chem. C* **2008**, *112*, 16521−16531.
(19) Kamala, C. R.; Ayappa, K. G.; Yashonath, S. Mutual Diffusion in A Binary Ar-Kr Mixture Confined Within Zeolite Nay. *Phys. Rev. E: Stat., Nonlinear, Soft Matter Phys.* **2002**, *65*, 061202.
(20) Kumar, N. A.; Gaddam, R. R.; Suresh, M.; Varanasi, S. R.; Yang, D.; Bhatia, S. K.; Zhao, X. Porphyrin−Graphene Oxide Frameworks for Long Life Sodium Ion Batteries. *J. Mater. Chem. A* **2017**, *5*, 13204−13211.
(21) Thornton, A. W.; Nairn, K. M.; Hill, A. J.; Hill, J. M. New Relation Between Diffusion and Free Volume: I. Predicting Gas Diffusion. *J. Membr. Sci.* **2009**, *338*, 29−37.
(22) Bousige, C.; Levitz, P.; Coasne, B. Bridging Scales in Disordered Porous Media by Mapping Molecular Dynamics Onto Intermittent Brownian Motion. *Nat. Commun.* **2021**, *12*, 1043.
(23) Neyertz, S.; Brown, D. A Trajectory-Extending Kinetic Monte Carlo (Tekmc) Method for Estimating Penetrant Diffusion Coefficients in Molecular Dynamics Simulations of Glassy Polymers. *Macromolecules* **2010**, *43*, 9210−9214.
(24) Neyertz, S.; Brown, D.; Pandiyan, S.; Van Der Vegt, N. F. Carbon Dioxide Diffusion and Plasticization in Fluorinated Polyimides. *Macromolecules* **2010**, *43*, 7813−7827.
(25) Robeson, L. M. Correlation of Separation Factor Versus Permeability for Polymeric Membranes. *J. Membr. Sci.* **1991**, *62*, 165−185.
(26) Freeman, B. D. Basis of Permeability/Selectivity Tradeoff Relations in Polymeric Gas Separation Membranes. *Macromolecules* **1999**, *32*, 375−380.
(27) Robeson, L. M. The Upper Bound Revisited. *J. Membr. Sci.* **2008**, *320*, 390−400.
(28) Robeson, L.; Freeman, B.; Paul, D.; Rowe, B. An Empirical Correlation of Gas Permeability and Permselectivity in Polymers and Its Theoretical Basis. *J. Membr. Sci.* **2009**, *341*, 178−185.
(29) Comesaña-Gándara, B.; Chen, J.; Bezzu, C. G.; Carta, M.; Rose, I.; Ferrari, M.-C.; Esposito, E.; Fuoco, A.; Jansen, J. C.; Mckeown, N. B. Redefining the Robeson Upper Bounds for CO2/CH4 and CO2/N2 Separations Using A Series of Ultrapermeable Benzotriptycene-Based Polymers of Intrinsic Microporosity. *Energy Environ. Sci.* **2019**, *12*, 2733−2740.
(30) Yang, Z.; Guo, W.; Mahurin, S. M.; Wang, S.; Chen, H.; Cheng, L.; Jie, K.; Meyer, H. M.; Jiang, D.-E.; Liu, G.; Jin, W.; Popovs, I.; Dai, S. Surpassing Robeson Upper Limit for CO2/N2 Separation With Fluorinated Carbon Molecular Sieve Membranes. *Chem* **2020**, *6*, 631−645.
(31) Han, Y.; Ho, W. W. Polymeric Membranes for CO2 Separation and Capture. *J. Membr. Sci.* **2021**, *628*, 119244.
(32) Barnett, J. W.; Bilchak, C. R.; Wang, Y.; Benicewicz, B. C.; Murdock, L. A.; Bereau, T.; Kumar, S. K. Designing Exceptional Gas-Separation Polymer Membranes Using Machine Learning. *Sci. Adv.* **2020**, *6*, No. Eaaz4301.
(33) Li, H.; Zhang, X.; Chu, H.; Qi, G.; Ding, H.; Gao, X.; Meng, J. Molecular Simulation On Permeation Behavior of CH4/CO2/H2S Mixture Gas in Pvdf At Service Conditions. *Polymers* **2022**, *14*, 545.
(34) Krishna, R. Diffusion of Binary Mixtures in Zeolites: Molecular Dynamics Simulations Versus Maxwell−Stefan Theory. *Chem. Phys. Lett.* **2000**, *326*, 477−484.
(35) Bashir, M. A.; Al-Haj Ali, M.; Kanellopoulos, V.; Seppälä, J.; Kokko, E.; Vijay, S. The Effect of Pure Component Characteristic Parameters On Sanchez−Lacombe Equation-Of-State Predictive Capabilities. *Macromol. React. Eng.* **2013**, *7*, 193−204.
(36) Mahmood, S.; Xin, C.; Lee, J.; Park, C. Study of Volume Swelling and Interfacial Tension of the Polystyrene−Carbon Dioxide−Dimethyl Ether System. *J. Colloid Interface Sci.* **2015**, *456*, 174−181.
(37) Dasgupta, S.; Rajasekaran, M.; Roy, P. K.; Thakkar, F. M.; Pathak, A. D.; Ayappa, K. G.; Maiti, P. K. Influence of Chain Length On Structural Properties of Carbon Molecular Sieving Membranes and Their Effects On CO2, CH4 and N2 Adsorption: A Molecular Simulation Study. *J. Membr. Sci.* **2022**, *664*, 121044.
(38) Roy, P. K.; Kumar, K.; Thakkar, f. M.; Pathak, A. D.; Ayappa, K. G.; Maiti, P. K. Investigations On 6fda/Bpda-Dam Polymer Melt Properties and CO2 Adsorption Using Molecular Dynamics Simulations. *J. Membr. Sci.* **2020**, *613*, 118377.
(39) Kiyono, M.; Williams, P. J.; Koros, W. J. Effect of Pyrolysis Atmosphere On Separation Performance of Carbon Molecular Sieve Membranes. *J. Membr. Sci.* **2010**, *359*, 2−10.

https://doi.org/10.1021/acs.jpcb.3c05661
J. Phys. Chem. B 2023, 127, 9841−9849

(40) Potoff, J. J.; Siepmann, J. I. Vapor−Liquid Equilibria of Mixtures Containing Alkanes, Carbon Dioxide, and Nitrogen. *AIChE J.* **2001**, *47*, 1676−1682.
(41) Mayo, S. L.; Olafson, B. D.; Goddard, W. A. Dreiding: A Generic force Field for Molecular Simulations. *J. Phys. Chem.* **1990**, *94*, 8897−8909.
(42) Plimpton, S.; Crozier, P.; Thompson, A. *Lammps-Large-Scale Atomic/Molecular Massively Parallel Simulator*; Sandia National Laboratories; 2007, Vol. *18*, p 43.
(43) Tien, W.-J.; Chiu, C.-C. Generic Parameters of Trajectory-Extending Kinetic Monte Carlo for Calculating Diffusion Coefficients. *AIP Adv.* **2018**, *8*, 065311.
(44) Mark, P.; Nilsson, L. Structure and Dynamics of the Tip3p, Spc, and Spc/E Water Models At 298 K. *J. Phys. Chem. A* **2001**, *105*, 9954−9960.
(45) Tsimpanogiannis, I. N.; Moultos, O. A.; Franco, L. F. M.; Spera, M. B. d. M.; Erdős, M.; Economou, I. G. Self-diffusion coefficient of bulk and confined water: a critical review of classical molecular simulation studies. *Mol. Simul.* **2019**, *45*, 425−453.
(46) Alexander Stern, S. Polymers for Gas Separations: The Next Decade. *J. Membr. Sci.* **1994**, *94*, 1−65.
(47) Peng, D.-Y.; Robinson, D. B. A New Two-Constant Equation of State. *Ind. Eng. Chem. Fundam.* **1976**, *15*, 59−64.
(48) Dubbeldam, D.; Calero, S.; Ellis, D. E.; Snurr, R. Q. Raspa: Molecular Simulation Software for Adsorption and Diffusion in Flexible Nanoporous Materials. *Mol. Simul.* **2016**, *42*, 81−101.
(49) Steel, K. M.; Koros, W. J. An Investigation of the Effects of Pyrolysis Parameters On Gas Separation Properties of Carbon Materials. *Carbon* **2005**, *43*, 1843−1856.
(50) Coudert, F.-X.; Jeffroy, M.; Fuchs, A. H.; Boutin, A.; Mellot-Draznieks, C. Thermodynamics of Guest-Induced Structural Transitions in Hybrid Organic−Inorganic Frameworks. *J. Am. Chem. Soc.* **2008**, *130*, 14294−14302.
(51) Kamala, C. R.; Ayappa, K. G.; Yashonath, S. Large Distinct Diffusivity in Binary Mixtures Confined To Zeolite Nay. *J. Phys. Chem. B* **2005**, *109*, 22092−22095.
(52) Baker, R. W.; Low, B. T. Gas Separation Membrane Materials: A Perspective. *Macromolecules* **2014**, *47*, 6999−7013.
(53) Jamali, S. H.; Bardow, A.; Vlugt, T. J. H.; Moultos, O. A. Generalized Form for Finite-Size Corrections in Mutual Diffusion Coefficients of Multicomponent Mixtures Obtained from Equilibrium Molecular Dynamics Simulation. *J. Chem. Theory Comput.* **2020**, *16*, 3799−3806.

https://doi.org/10.1021/acs.jpcb.3c05661
J. Phys. Chem. B 2023, 127, 9841−9849